Submitted for publication in *The Astrophysical Journal*

On the Non-Gaussianity observed in the *COBE*-DMR Sky Maps

A.J. Banday[1] and S. Zaroubi[2]

Max Planck Institut für Astrophysik, D-85740 Garching bei München, Germany.

and

K.M. Górski[3,4,5]

Theoretical Astrophysics Center, Juliane Maries Vej 30, DK-2100, Copenhagen 0, Denmark.

ABSTRACT

In this paper we pursue the origin of the non-Gaussianity determined by a bispectrum analysis of the *COBE*-DMR 4-year sky maps. The robustness of the statistic is demonstrated by the rebinning of the data into 12 coordinate systems. By computing the bispectrum statistic as a function of various data partitions – by channel, frequency, and time interval, we show that the observed non-Gaussian signal is driven by the 53 GHz data. This frequency dependence strongly rejects the hypothesis that the signal is cosmological in origin. A jack-knife analysis of the coadded 53 and 90 GHz sky maps reveals those sky pixels to which the bispectrum statistic is particularly sensitive. We find that by removing data from the 53 GHz sky maps for periods of time during which a known systematic effect perturbs the 31 GHz channels, the amplitudes of the bispectrum coefficients become completely consistent with that expected for a Gaussian sky. We conclude that the non-Gaussian signal detected by the normalised bispectrum statistic in the publicly available DMR sky maps is due to a systematic artifact. The impact of removing the affected data on estimates of the normalisation of simple models of cosmological anisotropy is negligible.

Subject headings: Cosmology: theory — observation — cosmic microwave background: tests of gaussianity

---

[1] *email:* banday@mpa-garching.mpg.de

[2] *email:* saleem@mpa-garching.mpg.de

[3] Warsaw University Observatory, Aleje Ujazdowskie 4, 00-478 Warszawa, Poland.

[4] Current address: ESO, D-85740 Garching bei München, Germany.

[5] *email:* kgorski@eso.org

1. Introduction

Gaussianity plays a fundamental role in modern physics. For a Gaussian field, the power spectrum tells us all there is to know about that field. In cosmology too, the role of Gaussian statistics is of great importance. Inflation (or at least the simplest models thereof) produces density perturbations which are random-phase and have amplitudes with a Gaussian distribution on any given scale. Since the onset of non-linear evolution for the density perturbations can itself create non-Gaussian correlations, it is simplest to test the statistics of the perturbations in the linear regime. Such scales are cleanly probed by anisotropies in the Cosmic Microwave Background (CMB) as imprinted by density perturbations on the last scattering surface.

Since 1992 (Smoot et al., 1992) the *COBE*-DMR maps of the microwave sky at 31.5, 53 and 90 GHz have been proferred as strong evidence in support of the inflationary paradigm. Many tests applied to the data have shown consistency with Gaussianity. For example, skewness and kurtosis (Smoot et al., 1994), the three-point correlation function (Hinshaw et al., 1994, 1995; Luo, 1994), the correlation function of temperature extrema (Kogut et al., 1995), the genus (Smoot et al., 1994; Colley, Gott & Park, 1996), a compendium of the above as applied to the 4-year sky maps (Kogut et al., 1996a), the bispectrum (Heavens, 1998) and Minkowski functionals (Schmalzing & Górski, 1998). Recent analyses by Pando, Valls-Gabaud & Fang (1998) using wavelets and Ferreira, Magueijo & Górski (1998) utilising a normalised bispectrum estimator find evidence for non-Gaussianity at levels of 98% or above[6]. Such a result is simply remarkable: even the major theoretical competitor to inflation – models which invoke networks of cosmological defects to seed structure formation – only show evidence of non-Gaussian CMB behaviour in subtle ways. In fact, one still expects the large-scale anisotropy seen by *COBE*-DMR for a typical defect model to appear quite Gaussian (as a consequence of the typical coherence scale of a defect being small relative to the DMR beam and an application of the central limit theorem). The detection of *cosmological* non-Gaussianity in the DMR data would have profound implications for all models of structure formation.

Before moving on to our own analysis, we would like to point out that we do not consider it correct to 'de-weight' the significance of the new results given that earlier tests failed to reject Gaussianity. In particular, non-Gaussianity has no generic signature on the sky, and as such different tests will demonstrate variable statistical power depending on the type of non-Gaussian feature being sought. For any statistic, there are relative merits and disadvantages depending on whether the non-Gaussian features are localised in Fourier or real space, the effective scales probed

---

[6]An additional paper by Novikov, Feldman & Shandarin (1999) applying partial Minkowski Functionals to the *COBE*-DMR DCMB and DSMB foreground removed sky maps has been cited by some as additional evidence for non-Gaussianity. However, they apply their analysis to the full sky which is simply incorrect given the known inadequacies of the foreground removal techniques. This results in several obvious residual artifacts, especially in the Galactic Center region. We point out that the authors themselves do not consider that their analysis has detected any significant non-Gaussianity.

by the statistic, and the impact of instrumental noise on the analysis (as a simple case, the skewness was shown to be biased by noise in Smoot et al., 1994). It is certainly possible that a model can appear Gaussian over many scales but then suddenly demonstrate very non-Gaussian behaviour.

In what follows, we will attempt to determine the origin of the non-Gaussian signal detected in the *COBE*-DMR 4-year sky maps using the bispectrum technique of Ferreira, Magueijo & Górski (1998 – hereafter FMG). After reviewing the statistic itself and summarising the current status of the bispectrum analysis, we will determine the stability of the computed bispectrum amplitudes as the data is rebinned into 12 different coordinate systems, investigate the presence of signal in various data partitions by channel and year, infer a region of the DMR sky to which the statistic is particularly sensitive, and finally propose a plausible origin of the detected signal based on a known systematic error.

2. The Bispectrum Statistic

In this section we consider the definition of a *normalised bispectrum* as defined in FMG. In the spherical harmonic representation one can expand the temperature field on the celestial sphere in terms of $a_{\ell m}$ coefficients,

$$\Delta T(\mathbf{n}) = \sum_{\ell m} a_{\ell m} Y_{\ell m}(\mathbf{n}) \tag{1}$$

If we consider a multipole coefficient of the field

$$\Delta T_\ell = \sum_m a_{\ell m} \tag{2}$$

then by forming the tensor product of 3 such coefficients and requiring rotational invariance one computes an estimator of the bispectrum as

$$\begin{aligned} \hat{B}_\ell &= \alpha_\ell \sum_{m_1 m_2 m_3} \mathcal{W}^{\ell\ell\ell}_{m_1 m_2 m_3} a_{\ell m_1} a_{\ell m_2} a_{\ell m_3} \\ \alpha_\ell &= \frac{1}{(2\ell+1)^{\frac{3}{2}}} \left(\mathcal{W}^{\ell\ell\ell}_{000}\right)^{-1} \end{aligned} \tag{3}$$

where $\mathcal{W}^{\ell_1 \ell_2 \ell_3}_{m_1 m_2 m_3}$ are the Wigner 3-J coefficients.

Finally, FMG require a statistic which is invariant under a parity transformation and dimensionless. They define I^3_ℓ to be

$$I^3_\ell = \left| \frac{\hat{B}_\ell}{(\hat{C}_\ell)^{3/2}} \right| \tag{4}$$

where $\hat{C}_\ell = \frac{1}{2\ell+1} \sum_m |a_{\ell m}|^2$ (ie. the power spectrum). This is the normalised bispectrum we refer to in what follows. Only EVEN values of ℓ lead to non-zero bispectrum amplitudes due to the properties of the Wigner 3-J coefficients.

The bispectrum coefficients are evaluated from an input sky map as follows. We apply the extended Galactic cut of Banday et al. (1997) to the sky map in order to excise those pixels with significant Galactic contamination near the plane of the Galaxy, subtract the best-fit monopole and dipole from the remaining pixels[7], then compute the harmonic amplitudes $a_{\ell m}$ according to eqn (1). (3) and (4) subsequently allow the bispectrum values to be determined. Monte Carlo simulations of the sky as seen by *COBE*-DMR are then used to compute the statistical distributions of the various I^3_ℓ modes, since these are themselves inherently non-Gaussian. The distributions are then compared to the data in order to assess statistical significance.

3. Summary of the Current Situation

The above method has been applied to the coadded 53 and 90 GHz *COBE*-DMR 4-year sky maps by FMG. Fig. 1 shows our results (for Galactic frame data) to be compared with the corresponding Figure in their paper. Clearly, we reproduce their results to high accuracy. The main features of the FMG results are as follows: based on a "χ^2"-like analysis of the bispectrum results FMG find that the DMR coadded 53 and 90 GHz data are inconsistent with Gaussianity at more than 98% c.l.; that this result is driven by the I^3_{16} mode; and that the bispectrum amplitudes are noise dominated beyond $\ell = 18$.

Possible objections to the statistical significance of the analysis or suggestions as to plausible non-cosmological sources of the non-Gaussian signal have been addressed in several papers by the same authors (Magueijo, Ferreira & Górski, 1998, 1999; Ferreira, Górski & Magueijo, 1999). To summarise:

- the result is not sensitive to assumptions about the cosmological model, noise properties of the data, Galactic cut or other details of the analysis
- systematic error templates show no comparable signal
- correcting for Galactic foreground contamination in the usual way actually increases the confidence level for rejection of Gaussianity to over 99%

The latter result is quite intriguing in itself. Intuitively, one might feel that the Galactic foregrounds are more likely to demonstrate non-Gaussian behaviour than the CMB, yet this does not appear to be the case. Presumably, any non-Gaussianity manifests itself on scales other than those measured here, or, as with cosmological defect models, in more subtle ways. More importantly, the increase in the confidence level for rejection of Gaussianity answers those skeptics who might consider the original detection to be unconvincing. Given the previously held belief of the pristine nature of the *COBE*-DMR data, we proceed to expand on the FMG analyses.

---

[7]Note that this differs slightly from the procedure of FMG where only the monopole is subtracted. We have checked that we recover the FMG bispectrum values when we also omit the dipole subtraction.

4. Stability of the Bispectrum Statistic

The issue of the stability of the bispectrum estimator is of paramount importance to the legitimacy of the detection of non-Gaussianity. The microwave data obtained by the *COBE*-DMR instruments are subjected to an initial form of data reduction, namely the construction of full-sky maps. This is an important step, since it compresses the information contained in a large data-stream into a more managable size. At this map-making step, various systematic error corrections are applied, and the data is essentially binned into pixels with a preferred orientation and geometry on the sky, depending on both the pixelisation scheme and coordinate reference frame adopted. The reader should consult White & Stemwedel (1992) for a description of the *COBE* Quadrilaterized Spherical Cube – hereafter quadcube – pixelisation scheme. Obviously, one attempts to choose a pixel size which samples the sky signal in a lossless fashion. It is certainly the case, however, that certain systematic and/or noise signals may add more coherently in particular coordinate frames. This is a consequence of the result that there is no unique one-to-one mapping of pixels from one frame to another, since the pixels are of finite size and themselves have specific geometries. In essence, the signal and noise are rebinned from one frame to another, but one would naturally expect a robust statistical estimator to render results essentially independently of the coordinate frame. FMG recognise this important issue and do compare results in the publicly available Galactic and Ecliptic frames showing them to be very consistent. We extend their analysis further by analysing an additional 10 coordinate frames.

This important test will also allow us to comprehensively assess the impact of two other aspects of the analysis. The most obvious feature in the full-sky maps is the Galactic plane emission which must be discarded from the analysis. Some small 'leakage' of the strong Galactic emission into pixels close to the plane will vary slightly in the different coordinate schemes thereby testing whether the detected signal is due to residual Galactic plane signal surviving the cut. More importantly, as a consequence of the necessity to excise pixels from the analysis, the $a_{\ell m}$ coefficients we substitute in equation (4) contain aliased signal due to the incomplete sky coverage. The geometry of the Galactic plane cut in a given coordinate system determines the relative aliases contributions from other ℓ modes. Thus we can determine whether the detected signal is a chance aliasing of signals from other modes [8].

Fig. 2 shows our 12 reference frames. 4 correspond to conventional coordinate schemes of astronomical relevence – Galactic, Ecliptic, Celestial and Supergalactic. The remaining 8 were designed to place the Galactic plane in specific orientations with respect to the quadcube faces and edges in an attempt to maximise the conspiracy between the pixelisation scheme inaccuracies and the effect of data omission in the analysis.

In Fig. 3 we present the results of our analysis for the coadded 53 and 90 GHz data. There

---

[8] Of course, this is one of the reasons why Monte Carlo simulations are used to assess the significance of the bispectrum amplitudes. These should account for the aliasing issue at least statistically.

is excellent consistency of the I^3_ℓ values for all coordinate frames, with the peak-to-peak scatter between frames less than ~ 0.3 per mode. This explicitly establishes the rotational invariance of the estimator. The I^3_{16} mode has a well-defined mean value inconsistent with Gaussian behaviour. We note, however, that there are coordinate frames where this observed bispectrum amplitude is less significant as evidence for non-Gaussian behaviour, but also those where the reverse is true[9]. This might be interpreted by some as indicating a lack of robustness in the statistic. We believe that the observed mean value is significant, and that the scatter can be due to some variation in aliasing in the different schemes. Simply put, the non-Gaussian signal itself is actually suppressed by an increased aliased contribution from Gaussian modes in some cases. The behaviour of the I^3_{16} mode is clearly very different from the others and indicative of a genuine non-Gaussian feature in the coadded sky map.

5. Channel Dependence of the Bispectrum Signal

In this section we initially attempt to isolate the observed bispectrum signature to a particular channel or frequency. One should keep in mind that the signal-to-noise of the statistic varies as (Number of Observations)$^{\frac{3}{2}}$, so that such attempts are hindered by lower sensitivity. Still, we do find some revealing properties of the data. In the remainder of the section, we concentrate on the I^3_{16} mode predominantly.

Fig. 4 shows a compilation of results for the 53 and 90 GHz channels. The most important feature is the large I^3_{16} amplitude associated with the 53 GHz signal maps. For the sum map, although there are variations from frame-to-frame, these are consistent with those seen for the coadded data, despite lower signal-to-noise. For the individual channels, the situation is less clear, particularly for the 53B sky maps where in no case would one claim a detection of non-Gaussianity. The 53A does seem to contain strong hints of such behaviour. The 90 GHz channels, however, show no unusual properties whatsoever. The most appealing inference to make, therefore, is that the bispectrum signal in the coadded sky map is dominated by the contribution from the 53 GHz channels. If this is indeed the case, then we are forced to conclude that the underlying non-Gaussian signal, whatever its origin, is non-cosmological. It is also unlikely that the signal is noise-related since the difference maps show little evidence for significant bispectrum amplitudes.

Despite the decreasing returns expected, we consider the Galactic sky maps generated by partitioning the data into yearly or two yearly sections to determine whether we can isolate the cause of the detected bispectrum signal to a particular time period. This analysis proved less revealing: there is little strong evidence of a noteworthy signal present in any maps for I^3_{16} (Fig. 5). In fact, many ℓ-modes show a large scatter from year-to-year. In an Appendix, we demonstrate via

[9]In order to assess the significance of any differences observed, we have performed simulations to demonstrate that the distribution of I^3_ℓ values is essentially independent of the coordinate frame. Thus we can simply compare bispectrum amplitudes computed in different frames.

simulations that this is reasonable for such noise-dominated sky maps.

6. Does the Bispectrum Signal have a Spatial Signature?

Having asserted that the observed I^3_{16} signal is principally associated with a single frequency, we now attempt to determine whether the effect can be isolated spatially. In other words, can we identify specific pixels or groups of pixels to which our statistic is sensitive? We apply a 'jack-knife' type analysis to the maps: for every pixel surviving the Galactic cut, we recompute the bispectrum amplitude after removing that pixel and its 4 nearest neighbours. To visualise this, we plot as a sky map the bispectrum amplitude such that the value at a given pixel corresponds to the I^3_ℓ amplitude on removal of that pixel and its neighbours. Fig. 6 shows results for the interesting $\ell = 16$ mode in three coordinate systems – Galactic, Ecliptic and System 1. The general pattern (which is consistent upon rotation of the various frames to Galactic) reflects the underlying $\ell = 16$ mode. Nevertheless, there are clusters of pixels to which the bispectrum shows enhanced sensitivity. In particular, there are standout features in the Northern hemisphere (located in Galactic coordinates on Face 0 of the quadcube). One should recall that this is the region where Pando et al. (1998) detect a non-Gaussian signal using a wavelet method, and also that Magueijo et al. (1999) suggest a localisation of the non-Gaussian signal to the Northern Galactic hemisphere. Fig. 6b shows the I^3_{16} amplitude directly as a function of removed pixel index. Again, we note that System 1 has a lower average value for the bispectrum amplitude. However, for each system, the mean amplitude is well defined with typically small scatter, but a few very large excursions which increase or reduce the bispectrum value dramatically. Other bispectrum values show similar global behaviour related to their progenitor ℓ modes, but with notably less sensitivity to localised pixel clusters. Interestingly, Bromley & Tegmark (1999) have suggested that removing a pixel centred on $b = 39.5^\circ$ and $l = 257^\circ$ (pixel 4845 in Galactic coordinates) plus its 4 nearest neighbours reduces the I^3_{16} bispectrum amplitude to a statistically insignificant level[10], and propose that this reflects on the robustness of the bispectrum estimator. Our results show indeed that there are pixels to which the bispectrum is sensitive, but that the amplitude can be both significantly enhanced as well as reduced. This implies that there is a real spatial distribution of pixels which is the cause of the interesting I^3_{16} signal.

As an additional remark, we respond to claims that the observed signal may show dependence to localised noise. We have repeated our analyses on the sky maps after 'cleaning' them, ie. after removing all power above $\ell = 40$ (which is almost entirely noise dominated) as computed on the full-sky. There is no significant change in any of our results after performing this procedure, which, combined with the spatial signature noted above, refutes at least in part this suggestion.

---

[10]In our analysis, this procedure reduces the observed bispectrum amplitude from 0.949 to 0.678.

7. Impact of a Known Systematic Effect

As a result of our jack-knife analysis, we have found tentative evidence for a distribution of pixels on the sky which the data is sensitive to. We now attempt to attribute this signal with a systematic effect present in the time-ordered-data (TOD). Since the pixels affected do not fully cover the sky, any potential contaminant in the TOD should have a periodicity less than the six-months required to map the celestial sphere completely.

The 'eclipse effect' is an orbitally modulated signal taking place for approximately two months every year around the June solstice when the *COBE* spacecraft repeatedly flies through the Earth's shadow. The 31 GHz channels are particularly adversely affected, with obvious trends in the TOD present (see Fig. 2 of Kogut et al., 1992) which are strongly correlated with several housekeeping signals relating to the spacecraft thermal and electrical properties. However, an attempt to model and correct the erroneous signal based on this correlation was only partially successful: the model removes only two-thirds of the anomalous signal in the 31GHz channels. Consequently, the 31 GHz sky maps do not include data taken during the eclipse season. Only very small effects were noted for the 53 and 90 GHz channels, which were therefore corrected by the empirical model. Kogut et al. (1996b) estimated that only 0.3 μK rms artifacts are introduced into these channels if the eclipse data is included. Nevertheless, there are several hints that the eclipse period may be responsible for the observed bispectrum signal.

Firstly, the 31 GHz channels in which the eclipse data are rejected are extremely well-behaved with respect to the bispectrum tests, yet when we perform a similar analysis of the 31A channel with the eclipse data included one observes a notable enhancement of the I^3_{16} mode. This is quite suggestive despite the observed amplitudes being comfortably Gaussian in both cases, and the signal-to-noise being quite low (Fig. 7).

Secondly, the region of sky predominantly affected by removing the eclipse data aligns quite well with those pixels to which the bispectrum is apparently sensitive. Fig. 8 shows the temperature difference between the coadded 53 and 90 GHz sky maps made both with and without the eclipse data.

We therefore proceed to remove the eclipse periods from the 53 and 90 GHz data and study its impact on the bispectrum calculation. Fig. 9 summarises the situation. We note that:

- there is a remarkable drop in the I^3_{16} mode for the 53A channel, so that it is now practically consistent with zero, ie very Gaussian, and similarly an important drop in the 53B channel
- the 90 GHz channels remain largely unaffected and therefore comfortably consistent with Gaussianity
- the coadded 53 and 90 GHz sky map is now fully consistent with Gaussianity.

The impact on the 53A channel is particularly dramatic, the crucial issue being whether such a change in the statistic's value can be more simply attributed to the no-eclipse maps being noisier. We have performed a large number of simulations of CMB skies with noise properties corresponding to the two situations here. There are almost no cases where such a precipitous drop in the I^3_{16} occurs: in 20000 simulations we find only two cases where I^3_{16} drops by ~ 0.8 when comparing the no-eclipse with eclipse simulations. In fact, a mere 195 simulations demonstrate a drop of 0.5. This should not seem surprising: in our previous analysis of the changes of I^3_{16} from a yearly map to 4-year sky map, we see no similar behaviour for any mode, although the change in the noise contribution is, in this case, much greater.

We further note that a coadded sky map constructed from 53 GHz channels excluding the eclipse months and 90 GHz data including this data also demonstrates a drop in the bispectrum amplitude, whereas the reverse combination does not. This supports our earlier claim that the non-Gaussian signal is strongly associated with a single frequency and thus non-cosmological.

Since FMG found that the bispectrum amplitude at $\ell = 16$ was enhanced after subtraction of the Galactic foreground model, we repeat our analysis after correcting the no-eclipse coadded sky map. Although once again, there is some small increase in the amplitude of the formerly spurious mode, it still remains perfectly consistent with the expectations of a Gaussian model for the CMB signal and instrumental noise[11]

8. Impact on Previous Cosmological Results

The impact of the data excision on other analyses of the DMR data, especially the power spectrum fits to cosmological models, should be investigated. Although a comprehensive reassessment of all of the models previously constrained by the *COBE*-DMR data is beyond the scope of this paper, we have recomputed fits to a pure power law model of initial perturbations as parameterised by Q_{rms-PS} and n. For an analysis of the coadded 53 and 90 GHz data in Galactic coordinates including the eclipse data, we find

$$\mathrm{Q_{rms-PS}} = 15.63^{+3.20}_{-2.56}\ \mu\mathrm{K}, \mathrm{n} = 1.22^{+0.23}_{-0.27}$$

$$\mathrm{Q_{rms-PS}}\,|_{\mathrm{n=1}} = 18.44^{+1.3}_{-1.2}\ \mu\mathrm{K}$$

If we exclude the eclipse data

$$\mathrm{Q_{rms-PS}} = 16.27^{+3.20}_{-2.88}\ \mu\mathrm{K}, \mathrm{n} = 1.15^{+0.29}_{-0.25}$$

$$\mathrm{Q_{rms-PS}}\,|_{\mathrm{n=1}} = 18.25^{+1.4}_{-1.3}\ \mu\mathrm{K}$$

---

[11]The coadded (53A) sky map has an I^3_{16} value of 0.949 (0.791) which falls to 0.522 (0.012) on excluding the eclipse data. If we correct the data with the best fitting Galactic foreground model, the corresponding numbers are 1.112 (0.840) falling to 0.527 (0.116). .

These results are summarised in Fig. 10. The change in the best fit model is consistent with an increase in the average noise level per pixel of $\sim 10\%$, and is comparable with the difference in fits between Galactic and Ecliptic frame data (cf. Table 1 of Górski et al., 1996). We consider that it is unlikely that fits to other cosmological models will be affected with any greater significance.

It will, of course, be interesting to determine whether the eclipse effect is responsible for the wavelet detection of non-Gaussianity, especially given that the effect is localised on Face 0 of the *COBE* quadcube. We defer this to later work.

9. Summary

We believe that we have proposed a convincing non-cosmological candidate responsible for the observed non-Gaussian signal in the *COBE*-DMR 4-year sky maps.. That this candidate is, in fact, a known systematic artifact in the data is not unreasonable. Although the 31 GHz channels were affected by the eclipse data in such an intrusive way that the exclusion of the data was warranted, its impact on the 53 GHz channels is more subtle, and only revealed by a new statistic sensitive to non-Gaussian signals in the data. Presumably, the source of the signal corresponds to that part of the eclipse effect that could not be removed from the 31 GHz channels. In any case, excluding the data from the 53 GHz channels removes the non-Gaussian behaviour. We conclude, therefore, that the non-Gaussianity present in the publicly released DMR 4-year sky maps is not cosmological in origin. Fortunately, it appears that for most cosmological issues, the presence of this artifact is of no importance: analysis of the coadded sky maps excluding the eclipse data provides fits to power-law cosmological models completely consistent with previous work.

We thank Gary Hinshaw for useful suggestions. We acknowledge the efforts of those contributing to the *COBE*-DMR and particularly recognise the map-making skills of Phil Keegstra.

A. Noise dependence of the Bispectrum Statistic

An important issue in our statistical analysis of the bispectrum values is the dependence of the statistic on the signal-to-noise ratio of the data. In particular, we are interested in two aspects: how the probability distributions are modified, and how much scatter in a given I_ℓ^3 value can occur, when considering maps with noise integrated from one year to four years and then to a coadded map. We have performed a large number of simulations ($\sim$ 20000) to assess this dependence. In particular, we simulate a noiseless CMB sky, then add noise corresponding to the 53A channel for 1-year, add a second year of noise to create an effective 2-year map, then similarly to create the equivalent of a 4-year sky, a 4-year 53 GHz sum map, and finally a 4-year coadded 53 and 90 GHz map. In this way, we specifically account for the effect of noise integration over the mission and its impact on the underlying bispectrum signal.

Since we have been primarily concerned with the I^3_{16} amplitude, we shall concentrate on this mode here. Interestingly, the 6 bispectrum probability distributions for the cases considered – from noiseless CMB sky to a coadded map – have essentially identical probability distributions (to the extent that plotting them would be superfluous). In fact, we have explicitly made use of this fact above, where we have compared the results from different maps and time-periods directly in all Figures. Here, we have shown that this is valid, and that a change in I^3_{16} value from one map to another can be simply interpreted against a single underlying probability function. However, whilst the statistical distribution for I^3_{16} and indeed for all bispectrum amplitudes at least out to $\ell = 30$ as considered in this paper, is essentially unchanged by varying noise contamination, it is by no means the case that the bispectrum amplitude for a single CMB realisation is unaffected by instrument noise.

In fact, it is common that, for a given CMB realisation, there is some scatter in the determined bispectrum amplitude with noise integration. To quantify this, we have considered the difference between both successive pairs of estimates of I^3_{16} (eg. between a simulated 2-year and 4-year map) and between the underlying CMB amplitude and successive estimates of I^3_{16}. In all cases, the rms difference is ~ 0.25, although the distributions of the differences are more peaked than Gaussian with slightly broader tails. Fig. 11 summarises our findings. A particular value of the I^3_{16} amplitude for the CMB sky can be enhanced or suppressed by the addition of noise. Nevertheless, it is not common for an initially large CMB I^3_{16} amplitude to be obscured by noise, nor a small CMB amplitude to be enhanced to a level suggestive of non-Gaussianity. In fact, in only 5% of the simulated cases do we find that there is a change in the I^3_{16} value of over 0.5 between the noiseless CMB case and the coadded sky map. Furthermore, only $\sim 0.7\%$ of the simulations have CMB values greater than 0.8 and coadded amplitudes less than 0.2, or the reverse.

REFERENCES

[]Banday, A.J., Górski, K.M., Bennett, C.L., Hinshaw, G., Kogut, A., Lineweaver, C.H., Smoot, G.F., & Tenorio, L. 1997, ApJ, 475, 393

[]Bennett, C.L., et al. 1996, ApJ, 464, L1

[]Bromley, B.C., & Tegmark, M. 1999, ApJ submitted

[]Colley, W.N. Gott, III, J.R., & Park, C. 1996, MNRAS, 281, L82

[]Ferreira, P.G., Magueijo, J., & Górski, K.M. 1998, ApJ, 503, 1 (FMG)

[]Ferreira, P.G., Górski, K.M., & Magueijo, J. 1998, in the Proceedings of the Rome 3K conference; astro-ph/9904073

[]Górski, K.M., Banday, A.J., Bennett, C.L., Hinshaw, G., Kogut, A., Smoot, G.F., & Wright, E.L. 1996, ApJ, 464, L11

[]Heavens, A.F. 1998, MNRAS, 299, 805

[]Hinshaw, G., Kogut, A., Górski, K., Banday, A.J., Bennett, C.L., Lineweaver, C., Lubin, P., Smoot, G.F., & Wright, E.L. 1994, ApJ, 431, 1

[]Hinshaw, G., Banday, A.J., Bennett, C.L., Górski, K.M., & Kogut, A. 1995, ApJ, 446, L67

[]Kogut, A., et al. 1992, ApJ, 401, 1

[]Kogut, A., Banday, A.J., Bennett, C.L., Hinshaw, G.F., Lubin, P., & Smoot, G.F. 1995, ApJ, 439, L29

[]Kogut, A., Banday, A.J., Bennett, C.L., Górski, K.M., Hinshaw, G., Smoot, G.F., & Wright, E.L. 1996a, ApJ, 464, L29

[]Kogut, A., et al. 1996b, ApJ, 470, 653

[]Luo, X. 1994, Phys. Rev. D, 49, 3810

[]Magueijo, J., Ferreira, P.G., & Górski, K.M. 1998, in the Proceedings of the Planck meeting, Santender 98; astro-ph/9810414

[]Magueijo, J., Ferreira, P.G., & Górski, K.M. 1999, in the Proceedings of COSMO98, Asilomar; astro-ph/9903051

[]Novikov, D., Feldman, H.A., & Shandarin, S.F. 1999, ApJ submitted

[]Pando, J., Valls-Gabaud, D., & Fang, L. 1998, Phys. Rev. Lett., 81, 4568

[]Schmalzing, J., & Górski, K.M. 1998, MNRAS, 297, 355

[]Smoot, G.F., et al. 1992, ApJ, 396, L1

[]Smoot, G.F., et al. 1994, ApJ, 437, 1

[]White, R.A & Stemwedel, S.W. 1992, in ADASS I, ed. Worrall, D.M., Biemesderfer, C., & Barnes, J., San Francisco, ASP, pp 379

This preprint was prepared with the AAS LaTeX macros v5.0.

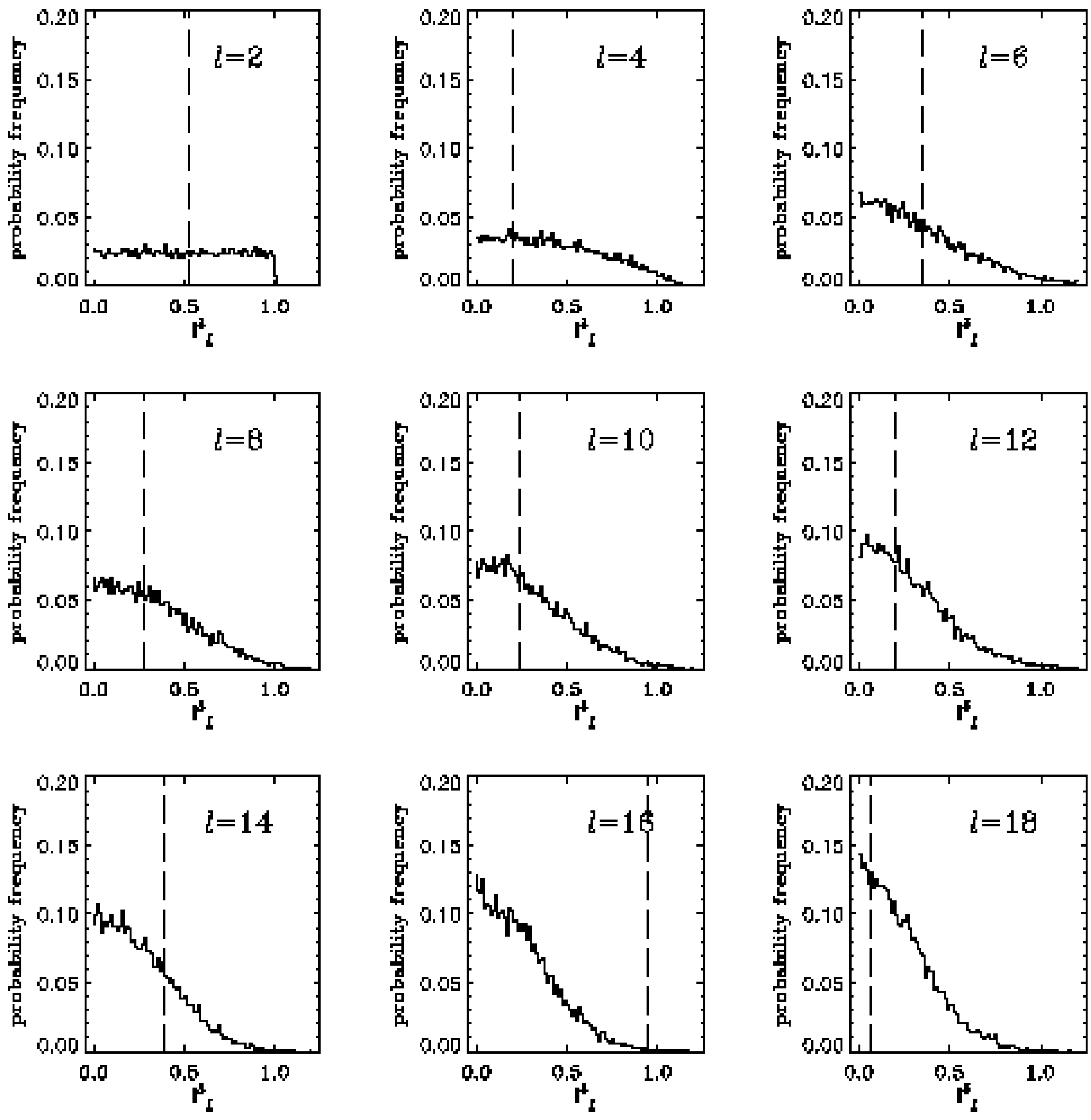

Fig. 1.— The probability distribution functions for the I_ℓ^3 statistic of a Gaussian CMB sky and random Gaussian noise appropriate to the coadded 53 and 90 GHz sky maps. Dashed line: the observed value of I_ℓ^3 for the coadded sky map in Galactic coordinates.

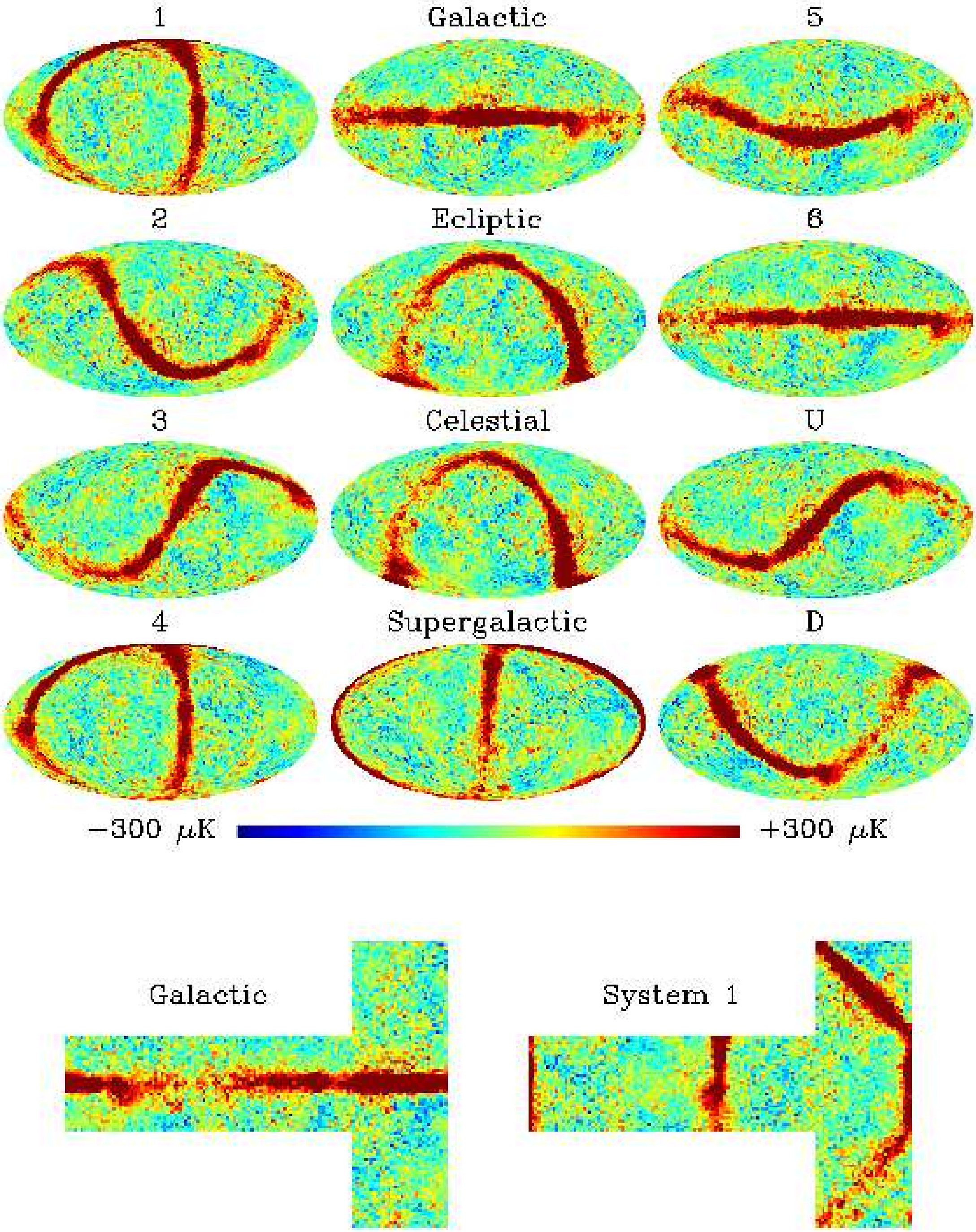

Fig. 2.— Upper: the coadded 53 and 90 GHz sky map in 12 different coordinate systems. The middle column corresponds to 4 reference frames of astronomical significance, the remaining 8 correspond to rotations of the sky designed to place the Galactic plane with specific geometries with respect to the underlying quadcube pixelisation scheme. Lower: the unfolded-T projection of the quadcube. The right-hand figure shows the rotated orientation of the Galactic plane relative to the left-hand figure.

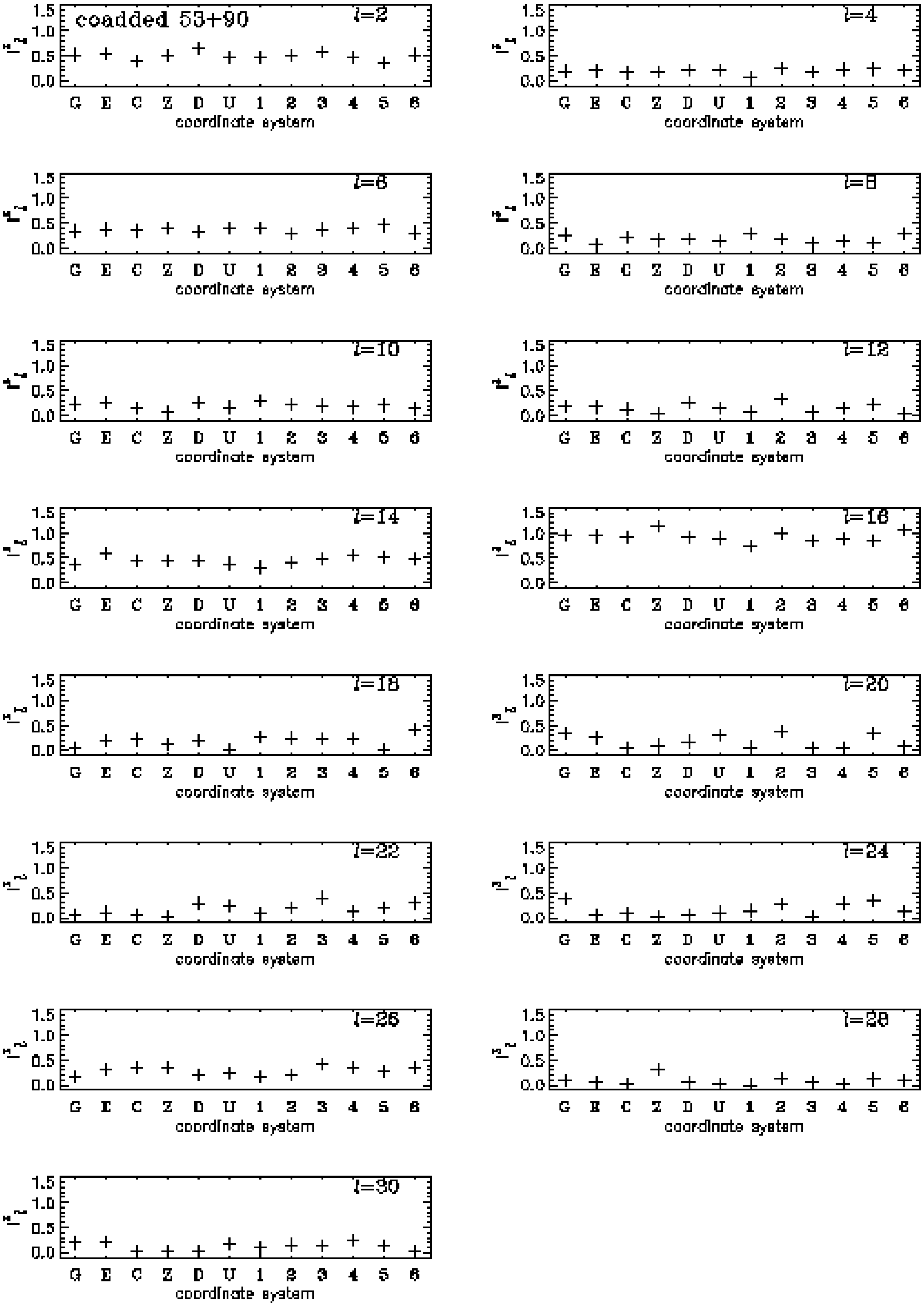

Fig. 3.— Variation of the I_ℓ^3 statistic computed with the coadded 53 and 90 GHz data for 12 coordinate systems. These include 4 astronomically important reference frames – Galactic (G), Ecliptic (E), Celestial (C) and Supergalactic (Z) – plus 8 others designed to place the Galactic plane in specific orientations with respect to the *COBE*-DMR quadcube.

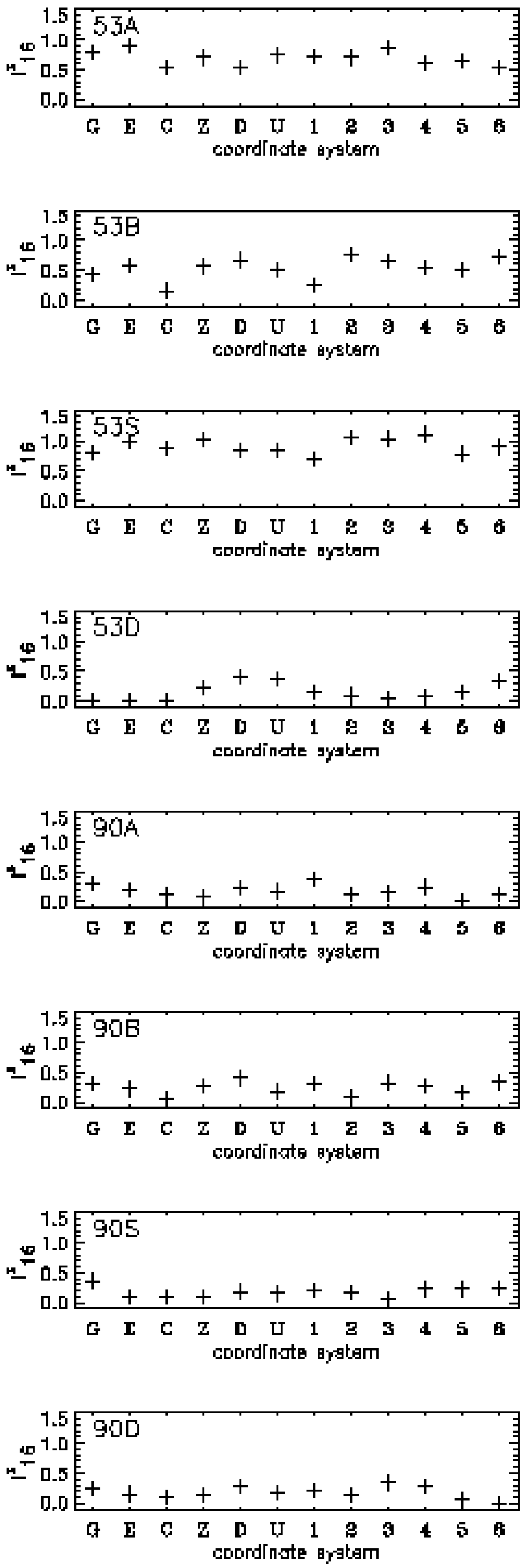

Fig. 4.— The I^3_{16} bispectrum amplitude for the 53A, 53B, 90A, 90B and their sum (S) and difference (D) maps as a function of our 12 coordinate systems.

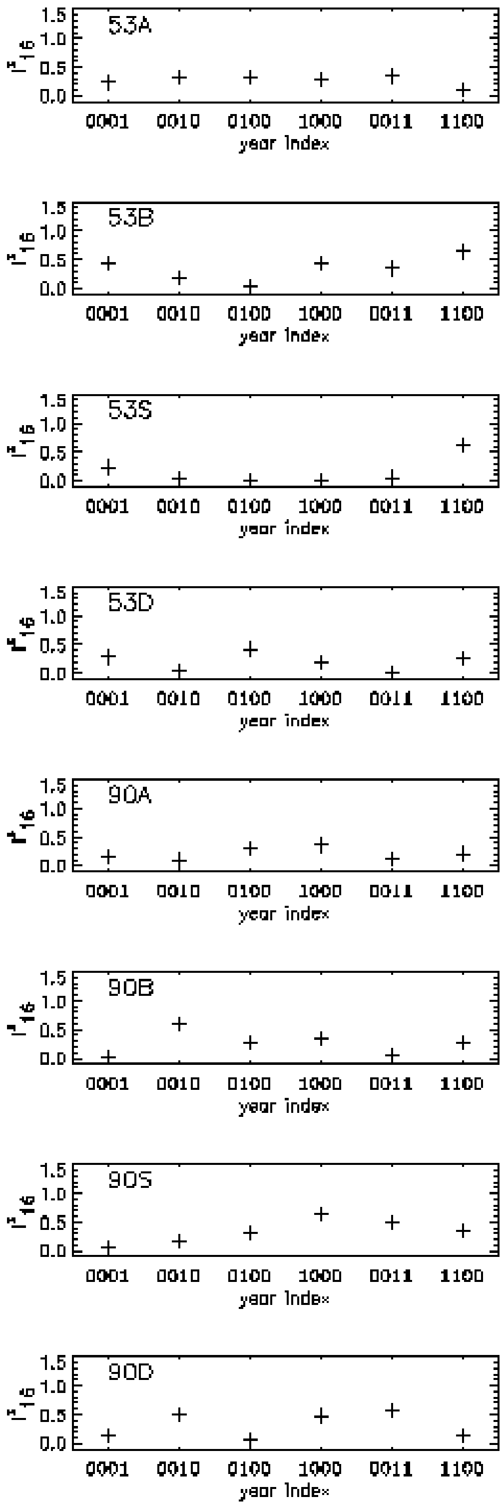

Fig. 5.— The 53 and 90 GHz I^3_{16} bispectrum amplitudes for the yearly and two-yearly Galactic sky maps. The index scheme is such that 0010 corresponds to the second year of data, 1100 to the third plus fourth years of data.

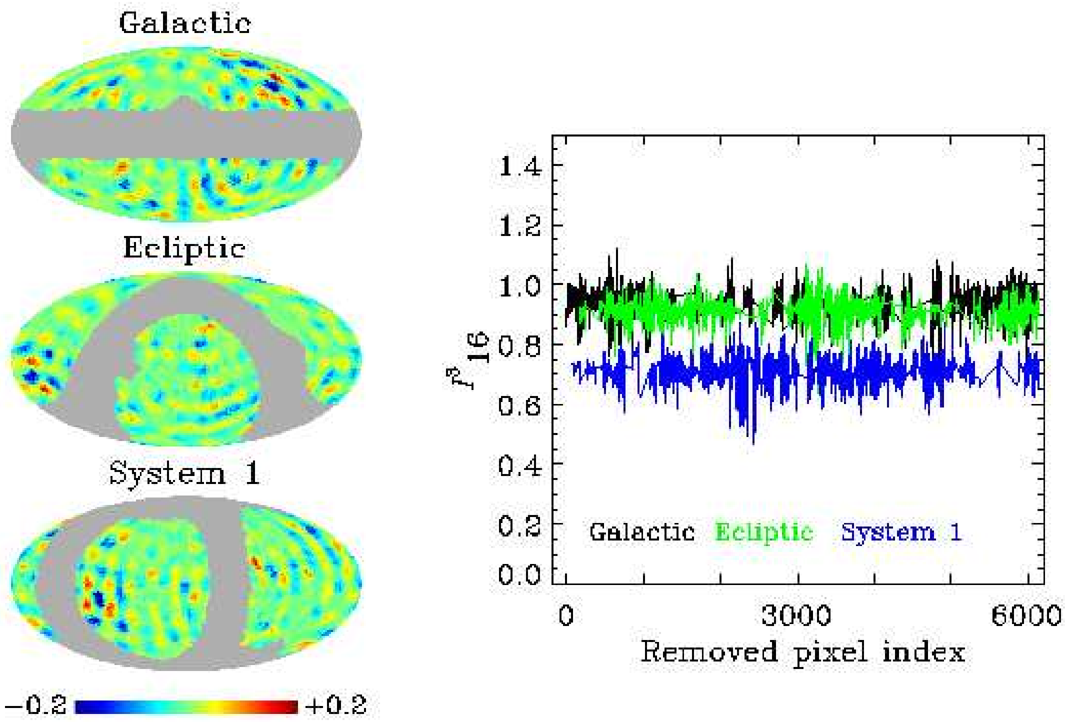

Fig. 6.— Results of the jack-knife analysis applied to the Galactic, Ecliptic and System 1 coadded sky maps. Note that the exclusion of various pixel groupings can both enhance and suppress the I^3_{16} bispectrum amplitude. The maps of the bispectrum amplitudes have had the mean value subtracted.

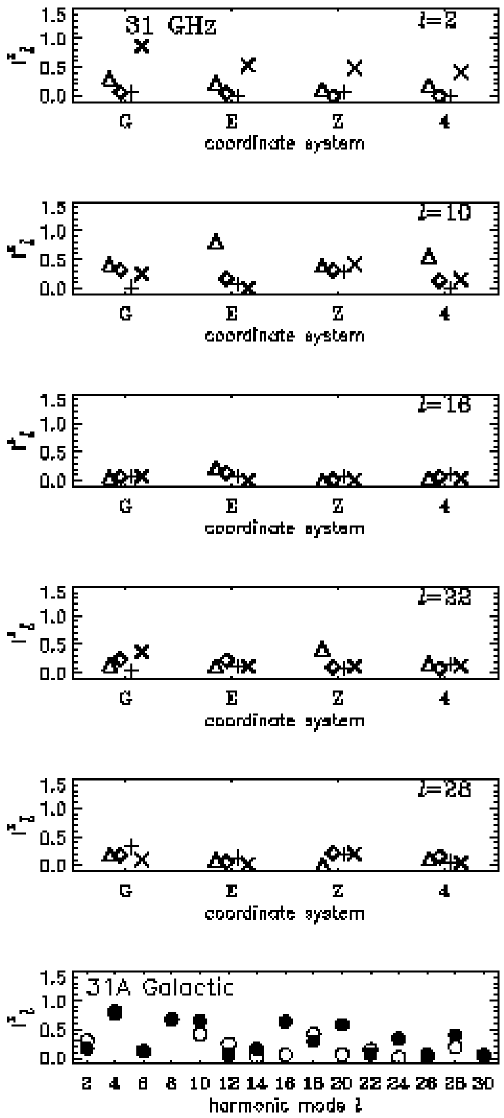

Fig. 7.— Top five panels: selected I_ℓ^3 amplitudes for the 31 GHz A,B sum and difference maps in 4 coordinate systems. Key: channel A = $\triangle$; channel B = $\diamond$; sum map = $+$; difference map = $\times$. Bottom panel: I_ℓ^3 for the 31A channel both excluding (open circles) and including (filled circles) the eclipse data. Note the marked increase at $\ell = 16$ when the eclipse data is included.

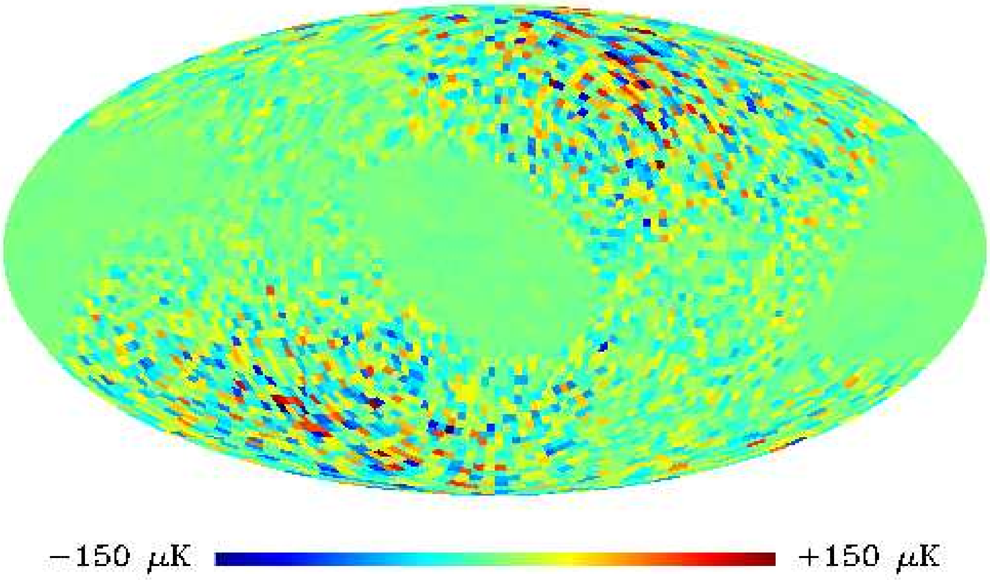

Fig. 8.— The temperature difference of the coadded sky maps in Galactic coordinates including and excluding the eclipse data.

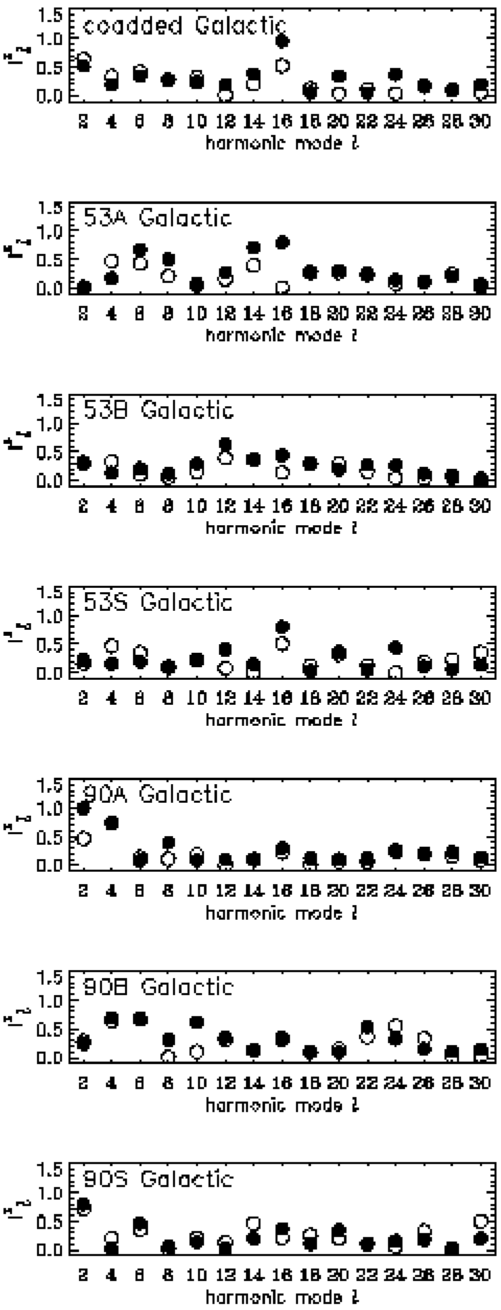

Fig. 9.— The I_ℓ^3 statistic for the coadded, 53 and 90 GHz A,B and sum (S) sky maps both including (filled circles) and excluding (open circles) the eclipse data.

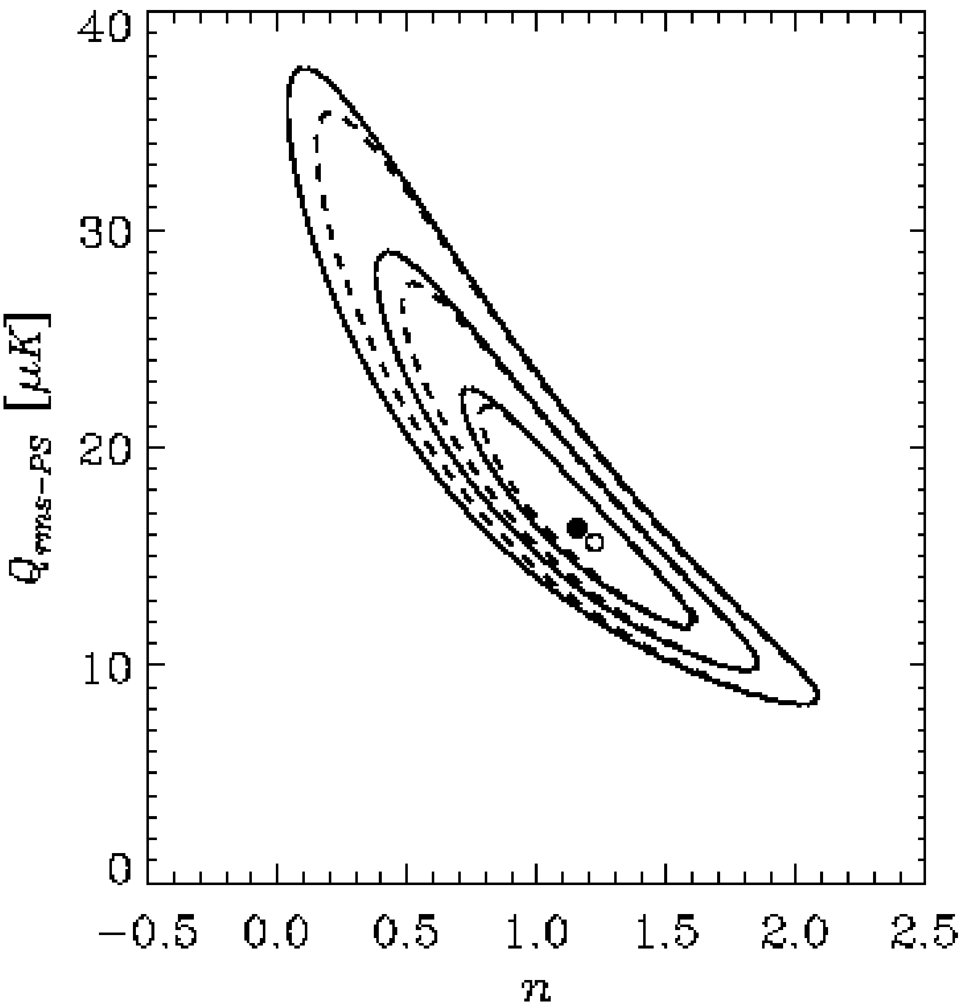

Fig. 10.— Results of fitting a simple power-law cosmological model, parameterised by a quadrupole normalisation Q_{rms-PS} and a spectral slope n, to the coadded 53 and 90 GHz Galactic sky maps. The dashed line corresponds to the fit including the eclipse data, the solid line excludes this period. The best-fit values are represented by the open circle when the eclipse period is included and the solid circle excluding this data. The shift in best-fit values is comparable to that seen between Galactic and Ecliptic sky maps.

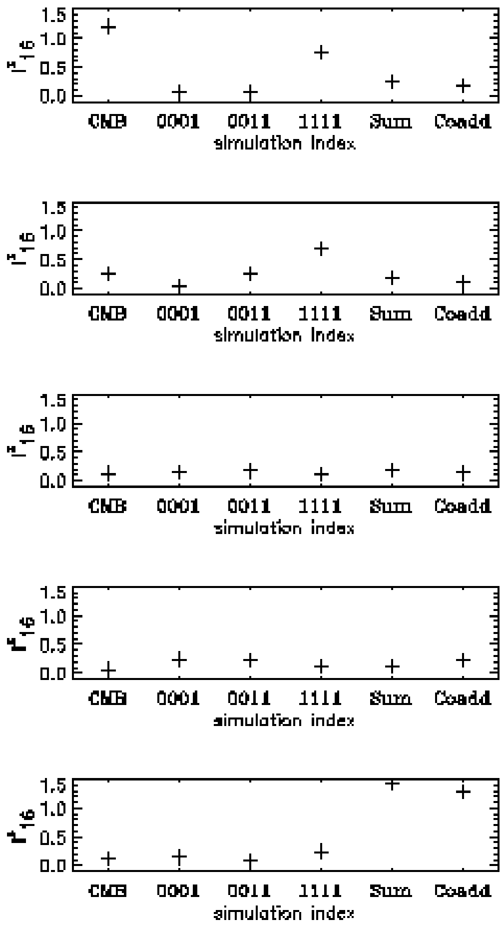

Fig. 11.— Simulations of the I^3_{16} bispectrum amplitude for an initial Gaussian CMB sky ('CMB') to which appropriate Gaussian noise levels are successively added to replicate the signal-to-noise properties of a 1-year 53A sky map ('0001'), a 2-year 53A sky map ('0011'), a 4-year 53A sky map ('1111'), a 53 GHz sum map ('Sum') and finally a coadded 53 plus 90 GHz sky map ('Coadd'). The top panel represents the worst case of differences between successive 'maps' for an initial CMB sky of large I^3_{16} value. The lowest panel shows the worst case when one is left with a coadded sky of large I^3_{16}. Some more typical variations are shown in between.